CIMS 2020

Proceedings of the
8th International Conference on
Coupled Instabilities in Metal Structures
Łodz University of Technology, Poland, July 12-14, 2021

Investigating local buckling in highly slender elliptical hollow sections through analysis of 3D-printed analogues

Finian McCann[1], Federico Rossi[2]

Abstract
Tubular structural members with slender cross-sections are susceptible to failure through local buckling of their tube walls. Previous numerical studies of steel elliptical hollow sections in compression predicted the local buckling modes and the ultimate loads of particularly slender specimens, with the results used to calibrate design methods for slender elliptical sections. Although these numerical parametric studies were conducted across a wide slenderness range, it was only possible to validate the models against experimental results in the low slenderness range since commercially available steel EHS are intended to satisfy non-slender geometric limits prescribed by structural design codes. Such limitations to the experimental scope are circumvented in the present study through testing of highly slender specimens produced using additive manufacturing techniques. A total of eight specimens of various cross-sectional aspect ratios and tube wall thicknesses were fabricated at London South Bank University using additive manufacturing techniques, which were then tested in compression; the observed load-deflection behaviour, ultimate loads, longitudinal strains and failure modes are discussed. Through appropriate rescaling of relevant parameters, design predictions for the ultimate load of the 3D-printed analogues are obtained using a design method intended for use with steel elliptical hollow sections. It is shown that the design predictions are safe-sided when compared to the present experimental results, with the accuracy generally increasing with aspect ratio and slenderness.

1. Introduction

Steel elliptical hollow sections (EHS) have found increased use in recent years in construction, having been employed in landmark projects such as Heathrow Terminal 5, Madrid Barajas Airport and Cork Airport (see Fig. 1a) (Chan et al, 2010). Such sections are characterized by their maximum outer cross-sectional diameter 2a, their minimum outer cross-sectional diameter 2b and their tube wall thickness t, as shown in Fig. 1b. The combination of the mechanical efficiency offered by having a greater major axis flexural resistance and the aesthetic appeal of elliptical geometry has been a factor in the increased popularity of EHS in steel construction (Ruiz-Teran & Gardner, 2008). Reflecting this increased usage, the sections are included in European structural specifications (Comité Européen de Normalisation, 2006) and the recent revision to EN 1993-1-1 (Comité Européen de Normalisation, 2018).

Studies into the behaviour of steel EHS are extensive, encompassing cross-section classification (Gardner & Chan, 2007), compressive resistance (Chan and Gardner, 2008a), bending resistance (Chan & Gardner,

[1] Senior Lecturer, London South Bank University, <mccannf@lsbu.ac.uk>
[2] Director of DARLAB, London South Bank University, <rossif@lsbu.ac.uk>

2008b), resistance in shear (Gardner et al, 2008), elastic buckling (Silvestre, 2008) and flexural buckling (Chan & Gardner, 2009). Studies have also been conducted on stainless steel EHS (Theofanous et al, 2009) and on cold-formed steel EHS (Chen & Young, 2020).

a)

b)

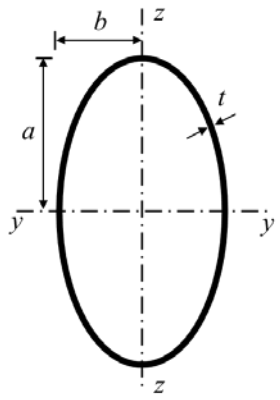

Figure 1: a) Steel EHS at Cork Airport; b) cross-sectional geometry of EHS showing dimensions and axes.

Studies into the local buckling of EHS conducted by Silvestre & Gardner (2011) and Insausti & Gardner (2011) characterized elastic buckling modes and postbucking behaviour. Leading from these previous studies, a numerical parametric study conducted by McCann et al (2016) confirmed that, with increasing aspect ratio a/b, the postbuckling behaviour of slender steel EHS in compression transitions from unstable imperfection-sensitive behaviour like that observed in cylindrical shells to stable imperfection-insensitive behaviour like that observed in flat plates. Although the numerical parametric study was conducted across a wide slenderness range, it was only possible to validate the models against experimental results from Chan & Gardner (2008a) in the relatively lower slenderness range since commercially available steel EHS are intended to satisfy non-slender geometric limits prescribed by structural design codes. In order to confirm that a design method proposed by McCann et al (2016) for slender EHS in compression is valid for use with cross-sections in the high slenderness range, it is appropriate that such highly slender specimens be tested. However, the required tube wall thickness would be too thin to fabricate or the outer dimensions too large to manipulate for testing.

In order to circumvent such issues, highly slender analogues fabricated from polymer using additive manufacturing techniques are investigated in the present study. In the context of structural engineering, additive manufacturing techniques have been primarily employed in the production of concrete-framed structures (Zhang et al, 2019), with other more limited applications in continuously-printed steel reinforcement (Paolini et al, 2019) and fibre-reinforced polymer formwork (Paolini et al, 2019); the world's first 3D-printed metal bridge was fabricated in the Netherlands in 2018 (de Zeen, 2018). Polymer structural components fabricated using additive manufacturing techniques offer advantages such as better environmental and corrosion resilience, greater precision and reliability, and, if recycled plastic is used, more sustainable structures. At present, the cost-effectiveness of using 3D-printed polymers in construction is hampered by production speeds and material strengths, but it is forecast that such limitations can be surmounted through advances in additive manufacturing and material science.

The objective of the present study is to examine the behaviour of highly slender steel elliptical hollow sections in compression through the use of polymer analogues fabricated using additive manufacturing techniques; the use of such techniques for educational purposes in structural mechanics has been

demonstrated successfully by Virgin (2018). An experimental campaign is described where EHS specimens of various cross-sectional aspect ratios and tube wall thicknesses are loaded in compression. Results for the ultimate load, the failure mode and the load–deflection behaviour are discussed. Comparison is made between the experimental ultimate loads and the design method for slender steel EHS proposed by McCann et al (2016), where it is found the design method provides safe-sided results with the accuracy increasing with aspect ratio and slenderness.

2. Experimental setup

In this section, the experimental campaign is described, including discussions on specimen geometry, the fabrication method, imperfections and the setup of the apparatus used in the experiments.

2.1 Geometry of EHS specimens

Eight additive-manufactured EHS specimens were fabricated at London South Bank University (LSBU) with cross-sectional aspect ratios a/b = 1.5, 2.0 and 3.0, and nominal tube wall thickness t between 1.5 mm and 3.0 mm. The specimens were labelled thus: EHS[specimen number]-[2a]-[2b]-[nominal t], e.g. Specimen 1 is labelled EHS01-100-50-3.0 (see Table 1). The maximum and minimum outer diameters of the sections were chosen so that the mean perimeter P_m is approximately constant for all specimens; the values of P_m and the cross-sectional area A calculated using the measured properties of the specimens are shown in Table 1. The nominal length L = 280 mm for all specimens, reflecting the maximum dimension producible by the printer used; this relatively short length also ensures that global buckling is precluded.

2.2 Additive manufacturing process

Geometric model files created using the nominal dimensions shown in Table 1 were used as input for an Ultimaker 3 Extended fused filament fabrication (FFF) printer based in the Digital Architecture Laboratory (DARLAB) at LSBU. The specimens were fabricated from filaments of polylactic acid (PLA) thermoplastic polymer with a nominal elastic modulus E = 2346.5 N/mm^2, a nominal yield strength of 49.5 N/mm^2 and a nominal fracture strain of 5.2% (Ultimaker, 2018); the finished specimens are shown in Fig. 2. Considering that the yield strain of S355 steel is 0.17% while that of PLA is 12.5 times higher at 2.1%, PLA sections exhibit a considerably greater elastic deformation capacity than steel sections and are hence more susceptible to failure initiating through buckling as opposed to inelastic effects.

Figure 2: Fabricated EHS stub specimens.

Given that extruded filaments of PLA were deposited about the circumference of the section, the fabrication process thus leads to a degree of anisotropy within the completed specimens, with the

circumferential material properties being greater than those in the longitudinal direction. It was found that the degree of anisotropy in the elastic modulus E, which governs local buckling, was minimal.

2.3 Precision of fabrication process

Prior to testing, the geometry of each specimen was measured in order to assess the level of deviation from the nominal dimensions. The outer diameters $2a$ and $2b$, and the specimen length L were found to be within 0.3% of the nominal values. Average wall thicknesses t are shown in Table 1 along with the standard deviations from the nominal dimensions. As can be seen, the coefficient of variation (COV) of t is between 2.4% and 4.0% for all specimens other than Specimen EHS08-105-35-1.5 where COV = 8.6%. When applying the design method of McCann et al (2016) in Section 4, the magnitude of the wall thickness imperfection Δw is assumed to be $0.05t$ for all specimens, which is comparable to the average imperfection magnitude of $\Delta w = 0.051t$ reported by Chan & Gardner (2008a) for steel EHS.

Table 1: Cross-sectional properties of specimens.

Specimen	a/b	Wall thickness t				P_m	A
		Nominal	Average	St.Dev	COV		
		(mm)	(mm)	(mm)	(mm)	(mm)	(mm^2)
EHS01-100-50-3.0	2.0	3.00	3.17	0.07	0.024	233	737
EHS02-90-60-2.0	1.5	2.00	2.07	0.05	0.027	232	478
EHS03-90-60-2.0	1.5	2.00	2.08	0.05	0.025	232	481
EHS04-90-60-2.0	1.5	2.00	2.04	0.05	0.025	232	473
EHS05-100-50-3.0	2.0	3.00	3.10	0.05	0.018	233	721
EHS06-100-50-1.5	2.0	1.50	1.45	0.06	0.040	238	344
EHS07-105-35-2.0	3.0	2.00	2.02	0.05	0.024	228	459
EHS08-105-35-1.5	3.0	1.50	1.39	0.13	0.086	230	344

2.4 Buckling of elliptical sections

The critical local buckling stress f_{cr} of an elliptical section is estimated by adapting the equivalent expression for a circular section:

$$f_{cr} = \frac{E}{\sqrt{3\left(1-\nu^2\right)}}\frac{2t}{D_{eq}} \tag{2}$$

where the Poisson's ratio $\nu = 0.35$ for PLA and the equivalent diameter $D_{eq} = 2(a^2/b)$; this value is twice the maximum radius of curvature in the elliptical section and reflects the point of initiation of buckling being at the extreme of the minimum radius. The slenderness parameter $\overline{\lambda}_\ell$ is defined as:

$$\overline{\lambda}_\ell = \sqrt{\frac{f_y}{f_{cr}}} \tag{3}$$

According to the classification limits prescribed by EN 1993-1-1 (CEN, 2018), an EHS in compression is classified as susceptible to local buckling if $D_{eq}/t\varepsilon^2 > 90$, where the material modification factor $\varepsilon = [(235/f_y)(E/210000)]^{0.5}$. The values of D_{eq}, $D_{eq}/t\varepsilon^2$, f_{cr} and $\overline{\lambda}_\ell$ calculated using the measured properties of the specimens are shown in Table 2. It should be noted that the maximum value of $D_{eq}/t\varepsilon^2$ found for the

steel EHS used to validate the model of McCann et al (2016) was 189, thus demonstrating the relatively high slendernesses being investigated presently.

Table 2: Buckling parameters calculated using measured properties.

Specimen	a/b	D_{eq} (mm)	$D_{eq} / t\varepsilon^2$	f_{cr} (N/mm^2)	$\overline{\lambda}_\ell$
EHS01-100-50-3.0	2.0	200	1189	45.9	1.04
EHS02-90-60-2.0	1.5	135	1233	44.2	1.06
EHS03-90-60-2.0	1.5	135	1225	44.5	1.05
EHS04-90-60-2.0	1.5	135	1246	43.8	1.06
EHS05-100-50-3.0	2.0	200	1216	44.8	1.05
EHS06-100-50-1.5	2.0	200	2603	20.9	1.54
EHS07-105-35-2.0	3.0	315	2948	18.5	1.64
EHS08-105-35-1.5	3.0	315	4281	12.7	1.97

2.5 Experimental method

Compression tests were conducted on the specimens in the Strength of Materials laboratory at London South Bank University. The specimen was placed in a Zwick/Roell 250 kN universal testing machine as shown in Fig. 3a; care was taken to position the specimens so that the load was applied as concentrically as possible in order to achieve an even stress distribution throughout the cross-section. A linear variable transducer (LVDT) was placed in contact with the upper loading platen in order to record the vertical displacement. Strain gauges were affixed to Specimen 1 at the positions indicated in Fig. 3b in order to measure the longitudinal strain (strain gauges were not affixed to the other specimens). The specimens were loaded in displacement control at a rate of 0.5 mm/min until failure.

a) b)

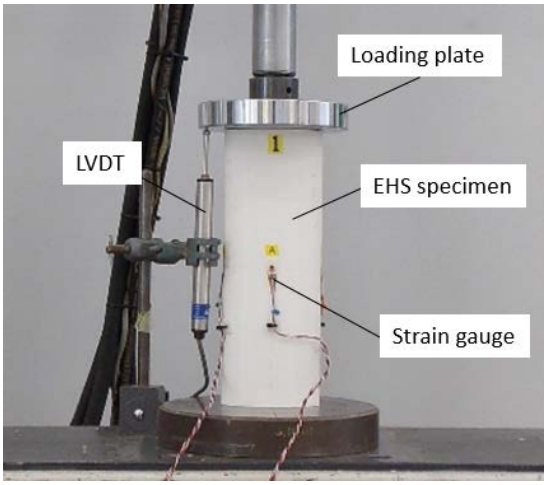

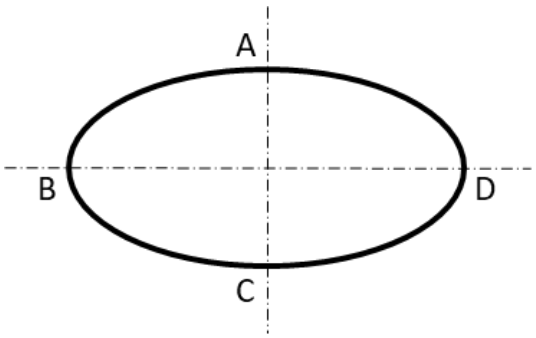

Figure 3: a) Specimen 1 in position for testing; b) locations of strain gauges at mid-height cross-section.

3. Experimental results

The load–displacement relationships recorded for each specimen are shown in Fig. 4, where it can be seen that each specimen underwent linear elastic deformation up to a sudden failure with a negligible amount of softening visible. The failure mode observed in each specimen involved sudden brittle ruptures initiating at the point of maximum radius of curvature, i.e., either point A or C in Fig. 3b. The

experimental ultimate load $N_{u,exp}$ for each specimen is compared with the fully-effective compressive resistance Af_y in Table 3 (the design predications for cross-sectional resistance $N_{c,Rd}$ discussed in Section 4 are also shown). It can be seen that the utilization of the full cross-sectional resistance diminishes with increasing slenderness, indicating that buckling had indeed occurred. Specimen EHS01-100-50-3.0 is shown post-failure in Fig. 5 – ruptures occurred at two cross-sections in each specimen tested.

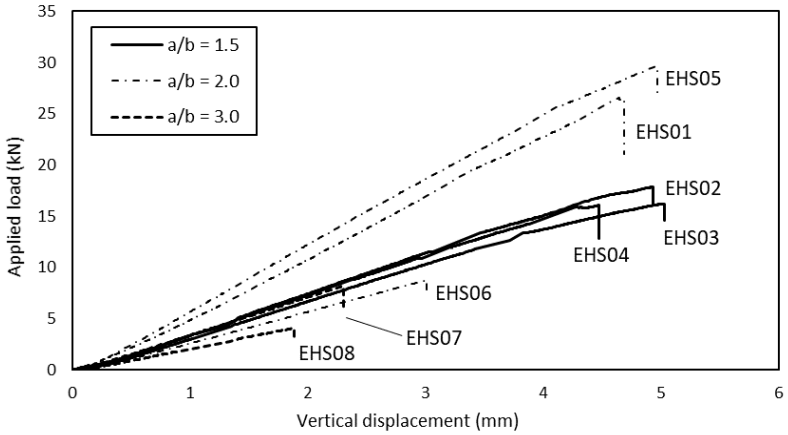

Figure 4: Load–displacement curves for all specimens.

Table 3: Experimental ultimate loads.

Specimen	a/b	$\overline{\lambda}_\ell$	Af_y (kN)	$N_{u,exp}$ (kN)	$N_{c,Rd}$ (kN)	$N_{u,exp} / Af_y$	$N_{u,exp} / N_{c,Rd}$
EHS01-100-50-3.0	2.0	1.01	36.5	26.6	19.1	0.73	1.39
EHS02-90-60-2.0	1.5	1.03	23.7	17.9	12.0	0.76	1.50
EHS03-90-60-2.0	1.5	1.03	23.8	16.2	12.1	0.68	1.34
EHS04-90-60-2.0	1.5	1.04	23.4	16.1	11.7	0.69	1.37
EHS05-100-50-3.0	2.0	1.03	35.7	29.7	18.5	0.83	1.61
EHS06-100-50-1.5	2.0	1.50	17.0	8.76	5.14	0.51	1.71
EHS07-105-35-2.0	3.0	1.60	22.7	8.22	7.10	0.36	1.16
EHS08-105-35-1.5	3.0	1.92	15.8	4.10	3.97	0.26	1.03

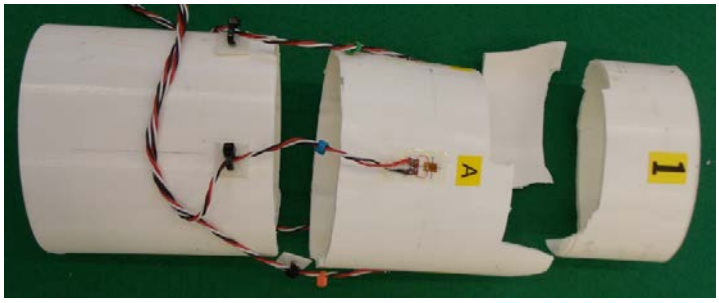

Figure 5: Specimen EHS01-100-50-3.0 post-failure.

The strains at mid-height are plotted against the average compressive stress in Fig. 6 for Specimen EHS01-100-50-3.0. It can be seen that the strain is higher at points A and C where the section is less stiff locally at the points of minimum curvature. The effective elastic modulus of the section calculated at point A is 2397 N/mm^2, a close approximation of the nominal value of 2346 N/mm^2.

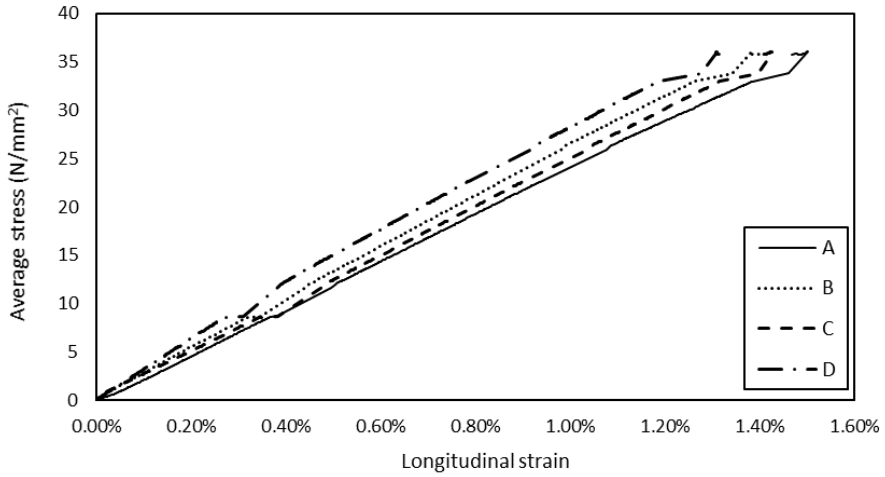

Figure 6: Longitudinal strains measured at the mid-height cross-section of Specimen EHS01-100-50-3.0.

4. Comparison with previous design method

The design method proposed by McCann et al (2016) is used to calculate a strength reduction factor ρ such that the design resistance in compression of EN 1993-1-1 (CEN, 2018) $N_{c,Rd} = \rho A f_y / \gamma_{M0}$; here, the material partial factor γ_{M0} is set equal to unity. The design method is not reproduced here in full; it suffices to say that it reflects the dependence of ρ on the local buckling slenderness, the aspect ratio a/b and the imperfection magnitude Δw. The calculated values of $N_{c,Rd}$ are shown in Table 3. In Fig. 7, design curves are plotted for a/b = 1.5, 2.0 and 3.0 with the imperfection magnitude $\Delta w = 0.05t$; the values for $N_{u,exp} / Af_y$ shown in Table 3 are also overlain. It can be seen that the design curves provide safe-sided predictions for all the experimental results with the accuracy generally increasing with aspect ratio and slenderness as also indicated by the values of $N_{u,exp} / N_{c,Rd}$ shown in Table 3.

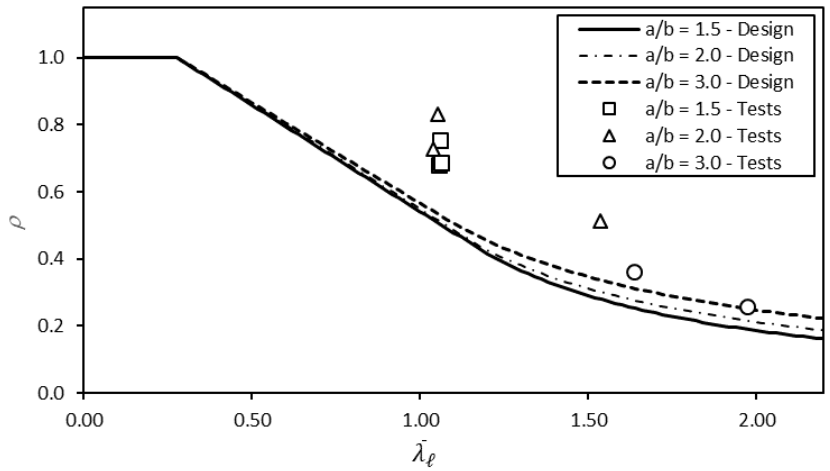

Figure 7: Comparison of experimental and design predictions for the local buckling reduction factor ρ.

5. Conclusions

A sample of eight elliptical hollow section specimens manufactured from polylactic acid polymer using the fused filament fabrication technique were tested in compression in order to assess their susceptibility to local buckling. It was found that, although the failure mode was brittle and very sudden, the results for ultimate load, failure mode and longitudinal strains indicate that local buckling occurred at the point of minimum curvature within the cross-sections. The experimental results for ultimate load

were compared with the predictions of an existing design method for slender steel elliptical hollow sections in compression. It was found that, upon rescaling the slenderness parameter to account for the change in material, the design method provided safe-sided predictions for the cross-sectional resistance for all specimens, with the accuracy increasing with aspect ratio and slenderness. This provides additional validation of the applicability of the design method for use with highly-slender specimens in various materials.

Acknowledgments
The authors wish to extend their thanks to Mr Paul Elsdon of the Strengths of Materials laboratory for conducting the experiments, and to Mr Ryan Lafferty for creating the specimen geometry models.

References

Comité Européen de Normalisation. (2006). *EN 10210-1:2006 Hot finished structural hollow sections of non-alloy and fine grain steels – Part 1: Technical delivery conditions*. British Standards Institution.

Comité Européen de Normalisation. (2018). *prEN 1993-1-1:2018 Final Draft - Eurocode 3 - Design of steel structures, Part 1.1: General rules and rules for buildings*, CEN.

Chan, T.M., Gardner, L. (2008). Compressive resistance of hot-rolled elliptical hollow sections. *Eng. Struct,* 30(2), 522–532.

Chan, T.M., Gardner, L. (2008). Bending strength of hot-rolled elliptical hollow sections, *J. Const. Steel Res.*, 64(9), 971–986.

Chan, T.M., Gardner, L. (2009). Flexural buckling of elliptical hollow section columns, *J. Struct. Eng., ASCE*, 135(5), 546–557.

Chan, T.M., Gardner, L., Law. K.H. (2010). Structural design of elliptical hollow sections: a review, *Proc. Inst. Civil Eng. – Struct. Build.* 163 (6), 391–402.

Chen, M.T., Young, B. (2020). Beam-column tests of cold-formed steel elliptical hollow sections, *Eng. Struct*, 210 10991.

De Zeen (2018). "World's first 3D-printed steel bridge unveiled at Dutch Design Week", online article available at www.dezeen.com/ published 22 October 2018.

Gardner, L., Chan, T.M. (2007). Cross-section classification of elliptical hollow sections. *Steel & Comp. Struct*, 7(3):185–200.

Gardner, L., Chan, T.M, Wadee, M.A. (2008). Shear response of elliptical hollow sections, *Proc. Inst. Civil Eng. – Struct. & Build.*, 161(6):301–309.

Insausti, A., Gardner, L. (2011). Analytical modelling of plastic collapse in compressed elliptical hollow sections. *J. Const. Steel Res.*, 67:678–89.

McCann, F., Fang, C., Gardner, L., Silvestre, N. (2016). Local buckling and ultimate strength of slender elliptical hollow sections in compression, *Eng. Struct.*, 111, 104–118.

Paolini, A., Kollmannsberger, S., Rank, E. (2019). Additive manufacturing in construction: a review on processes, applications, and digital planning methods, *Additive Manufacturing*, 30, 100894.

Ruiz-Teran, A.M., Gardner, L. (2008). Elastic buckling of elliptical tubes, *Thin-Walled Struct*. 46 (11) (2008) 1304–1318.

Silvestre, N. (2008). Buckling behaviour of elliptical cylindrical shells and tubes under compression, *Intl. J. Solids & Struct.,* 45(16):4427–4447.

Silvestre, N., Gardner, L. (2011). Elastic local postbuckling of elliptical tubes, *J. Const. Steel Res.,* 67(3):281–292.

Theofanous, M., Chan, T.M., Gardner, L. (2009). Structural response of stainless steel oval hollow section compression members, *Eng. Struct.*, 31(4):922–34.

Ultimaker. (2018). UM180821 TDS PLA RB V11 Technical data sheet PLA. Ultimaker.

Virgin, L. (2018). Enhancing the teaching of elastic buckling using additive manufacturing, *Eng. Struct.*, 174:338–345.

Zhang, J., Wang, J., Dong, S., Yu, X., Han. B. (2019). A review of the current progress and application of 3D printed concrete. *Composites Part A: Appl. Sci, & Manuf.*, 125.